LISA Pathfinder test-mass charging during galactic cosmic-ray flux short-term variations

2015 Class. Quantum Grav. 32 035001

(http://iopscience.iop.org/0264-9381/32/3/035001)

IOP Publishing Classical and Quantum Gravity
Class. Quantum Grav. **32** (2015) 035001 (14pp) doi:10.1088/0264-9381/32/3/035001

LISA Pathfinder test-mass charging during galactic cosmic-ray flux short-term variations

C Grimani[1,2], M Fabi[1], A Lobo[3,5], I Mateos[3] and D Telloni[2,4]

[1] DiSBeF, Università degli Studi di Urbino Carlo Bo, Urbino (PU), Italy
[2] Istituto Nazionale di Fisica Nucleare, Florence, Italy
[3] Institut de Ciències de l'Espai (CSIC-IEEC), Barcelona, Spain
[4] Istituto Nazionale di Astrofisica, Osservatorio Astrofisico di Torino, Pino Torinese, Italy

E-mail: catia.grimani@uniurb.it

Received 13 September 2014
Accepted for publication 8 October 2014
Published 5 January 2015

Abstract

Metal free-floating test masses aboard the future interferometers devoted to gravitational wave detection in space are charged by galactic and solar cosmic rays with energies > 100 MeV/n. This process represents one of the main sources of noise in the lowest frequency band ($< 10^{-3}$ Hz) of these experiments. We study here the charging of the LISA Pathfinder (LISA-PF) gold-platinum test masses due to galactic cosmic-ray (GCR) protons and helium nuclei with the Fluka Monte Carlo toolkit. Projections of the energy spectra of GCRs during the LISA-PF operations in 2015 are considered. This work was carried out on the basis of the solar activity level and solar polarity epoch expected for LISA-PF. The effects of GCR short-term variations are evaluated here for the first time. Classical Forbush decreases, GCR variations induced by the Sun rotation, and fluctuations in the LISA-PF frequency bandwidth are discussed.

Keywords: gravitational radiation detectors, solar cycles, cosmic rays, interplanetary propagation
PACS numbers: 95.55.Ym, 96.60.qd, 96.50.sb, 96.50.sh

(Some figures may appear in colour only in the online journal)

[5] Deceased.

1. Introduction

In November 2013, the European Space Agency selected the *Gravitational Universe* as one of its cornerstone science themes. In particular, eLISA [1, 2] is supposed to be the first interferometer devoted to gravitational wave detection in space operating in the frequency interval 10^{-4}–1 Hz. LISA Pathfinder (LISA-PF) [3, 4], the technology testing mission for eLISA, consists of one satellite carrying two gold-platinum free-floating test masses. LISA-PF will collect data for six months in 2015 orbiting about the L1 Lagrange point. Test-mass charging due to galactic and solar energetic particles (SEPs) [5, 6] represents one of the main sources of noise for the LISA-PF and eLISA missions [7].

The cosmic-ray composition in space consists approximately of 90% protons, 8% helium nuclei, 1% heavy nuclei, and 1% electrons [8]. The effects of cosmic rays on gravitational-wave experiments was considered in the past for ground-based detectors (e.g., [9–13] among others). However, cosmic-ray ground composition is made essentially of muons and therefore mission-customized studies must be carried out for space interferometers. More generally, a careful study of the environmental effects on the future space mission performance is more than recommended (see also [14] for the METIS coronagraph aboard the Solar Orbiter).

The minimum energy of protons and ions penetrating and charging the LISA-PF test masses is 100 MeV(/n). The expected role of electrons in 2015 was recently discussed in [15].

The integral flux of protons and helium nuclei at energies larger than the nominal cut-off energy of 70 MeV/n will be monitored with particle detectors hosted onboard LISA-PF [16, 17]. This conservative choice was made to not underestimate the overall particle flux charging the test masses and to consider the particle energy losses in the spacecraft material surrounding the radiation monitor at the occurrence of SEP events.

In this paper, we estimate the LISA-PF test mass charging due to galactic cosmic-ray (GCR) protons and helium nuclei during the mission operations (see also [18]). Variations and fluctuations of the charging process due to GCR short-term variations are discussed here for the first time.

The most intense short-term variations of GCR intensity occur during classical, non-recurrent Forbush decreases (FDs). Discovered by Scott Forbush in 1937 [19], these energy-dependent GCR intensity depressions follow the passage of interplanetary counterparts of coronal mass ejections. The maximum drop of cosmic-ray intensity is about 30% at 100 MeV/n. The FDs appear often mitigated below a few hundreds of MeV by a residual component of energetic particles of solar origin. GCR variations and fluctuations due to Sun rotation and other interplanetary processes are also considered.

The LISA-PF test mass charging simulations are carried out with the Fluka Monte Carlo package [20, 21]. The role of GCR nuclei with charge $Z > 2$ and that of interplanetary electrons with respect to protons can be inferred from Grimani *et al* [6, 15, 22].

For completeness, we add that SEP events characterized by proton differential fluxes above 100 MeV(/n) overcoming, by a few orders of magnitude, the overall GCR intensity may occur during the mission operations. These SEP events would generate a rapid increase of the test-mass charging. A maximum number of three intense events is expected during the second half of 2015 [18]. The radiation monitor aboard LISA-PF will allow us to follow the dynamics of SEP events, including the possibility to estimate the solar particle spatial distribution [23]. In the following, we show that the LISA-PF particle detector data can be also used to study the GCR flux variations characterized by minimum periodicities of 30 min or 1 h on the basis of the GCR intensity that will be observed after the launch of LISA-PF.

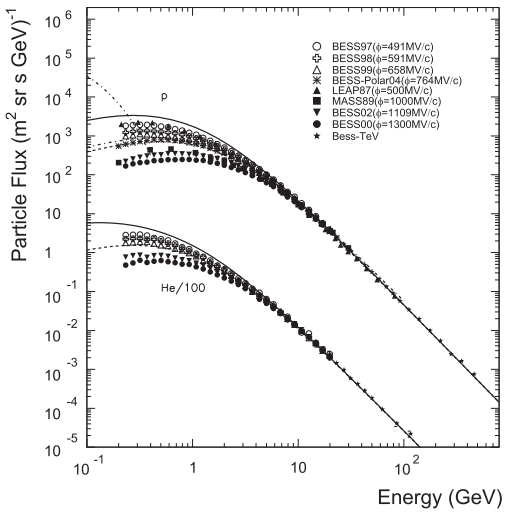

Figure 1. Estimated GCR proton and helium nuclei energy spectra during the second half of 2015. Maximum (solid lines) and minimum (dashed lines) projections are reported. Helium data are scaled by a factor of 100 in order not to superpose data and lines. The dot-dashed curves represent the proton flux observed by the PAMELA experiment during the FD of 14 December 2006 between 1650 and 2235 UT [30]. Galactic (bottom dot-dashed line) and solar (top dot-dashed line) proton components appear separated.

2. GCR proton and helium energy spectra in 2015

The second half of solar cycle 24 [24] will be characterized by a positive polarity epoch and a modest level of solar activity. We recall that a solar positive (negative) polarity period occurs when the global solar magnetic field lines exit from the Sun's North (South) Pole. The last change of solar polarity from − to + occurred at the end of 2013 [25]. Minimum, average, and maximum sunspot number (SSN) projections during the second half of 2015 are 27, 51, and 74, respectively [24].

In Grimani *et al* [26], it was found that during positive polarity periods the energy spectra, $J(r, E, t)$, of cosmic rays at a distance r from the Sun at a time t are well represented by the symmetric model in the force field approximation by Gleeson and Axford [27], assuming time-independent interstellar intensities $J(\infty, E + \Phi)$ and an energy loss parameter Φ:

$$\frac{J(r, E, t)}{E^2 - E_0^2} = \frac{J(\infty, E + \Phi)}{(E + \Phi)^2 - E_0^2} \tag{1}$$

where E and E_o represent the particle total energy and rest mass, respectively.

For Z = 1 particles with rigidity (particle momentum per unit charge) larger than 100 MV/c, the solar modulation level is completely defined by the solar modulation parameter ϕ that at these energies is equal to Φ [28]. By applying this model to the interstellar energy spectra estimated by Shikaze *et al* [29], we obtain the proton and helium nuclei energy differential fluxes during the LISA-PF operations in space, shown in figure 1. Continuous and dashed curves represent projections associated with the minimum (SSN = 27; ϕ = 350 MV/c) and maximum (SSN = 74; ϕ = 800 MV/c) levels of expected solar modulation intensities, respectively. The correlation between expected SSN in 2015 and solar modulation parameter

Table 1. Parameterizations of proton and helium energy spectra when LISA-PF will be sent into orbit. Minimum (m) and maximum (M) projections are considered.

	A_m	b_m	α_m	β_m	A_M	b_M	α_M	β_M
p	18000	1.54	3.67	0.88	18000	0.88	3.68	0.89
He	850	0.91	3.60	0.85	850	0.7	3.23	0.48

Table 2. ^{3}He/^{4}He ratio parameterization for the expected minimum level of solar modulation during the LISA-PF operations. The energy E is measured in GeV/n.

	$0.10 \leqslant E < 0.36$	$0.36 \leqslant E < 1.00$	$1.00 \leqslant E < 1.40$	$E \geqslant 1.40$
$C(350)$	$0.335 \times E^{0.569}$	0.187	$0.187 \times E^{0.491}$	0.22

Table 3. Same as table 2 for the expected maximum level of solar modulation in 2015.

	$0.10 \leqslant E < 0.30$	$0.30 \leqslant E < 0.80$	$0.80 \leqslant E < 2.50$	$E \geqslant 2.50$
$C(800)$	$0.239 \times E^{0.538}$	0.125	$0.140 \times E^{0.496}$	0.22

was carried out based on the work by Usoskin *et al* [31] where the monthly solar modulation parameter was estimated between 1951 and 2004. Minimum and maximum solar modulation parameter values during LISA-PF were set based on of the estimates of this same parameter in the past years when similar levels of solar activity were observed.

To simulate the charging process of the LISA-PF test masses, we have parameterized the proton and helium energy spectra expected in 2015. The interpolation function we used is reported next (see [8] for details):

$$F(E) = A\,(E + b)^{-\alpha}\,E^{-\beta} \quad \text{Particles/(m}^2\ \text{sr s GeV)} \tag{2}$$

where E is the particle kinetic energy per nucleon. The parameters A, b, α, and β appear in table 1.

The proper ^{3}He/^{4}He fraction in cosmic rays is considered in the simulations. The parameterizations of the ^{3}He/^{4}He ratio (see [6] for details), shown in tables 2 and 3, were carried out based on the minimum and maximum solar modulation intensities expected when LISA-PF will be in space. Recent data published on the ^{3}He/^{4}He ratio by the PAMELA [32] and BESS-Polar I experiments [33] are consistent with previous measurements. By indicating with C the ^{3}He/^{4}He ratio, with F (^{3}He) and F (^{4}He) the ^{3}He and ^{4}He energy differential fluxes and, finally, with F(He) the overall He flux, it is possible to find that

$$F\left(^3\text{He}\right) = [C/(1 + C)]\,F(\text{He}) \quad \text{Particles}\Big/\left(\text{m}^2\ \text{sr s GeV}\right) \tag{3}$$

$$F\left(^4\text{He}\right) = [1/(1 + C)]\,F(\text{He}) \quad \text{Particles}\Big/\left(\text{m}^2\ \text{sr s GeV}\right). \tag{4}$$

The test-mass charging due to ^{3}He and ^{4}He nuclei was determined by properly normalizing the overall He flux shown in figure 1 according to equations (3) and (4), respectively.

3. Forbush decreases

An FD is a drop of the GCR intensity. The most intense, sporadic events present a sudden onset and reach the minimum in approximately 1 d, whereas the recovery phase lasts from several days to a few weeks. Since the 1950s, FDs were detected regularly by neutron monitors as decreases ranging from a few percent up to 25% in the neutron monitor energy range (see [34]). Studies of FDs were also carried out using ground-level muon telescopes [35]. Systematic studies of intensity, shape, and recovery time versus energy are reported in [36] and references therein. To study the effects of an FD on the test-mass charging aboard LISA-PF, precise knowledge of the proton energy differential flux during the evolution of the event is required. Neutron and muon ground measurements do not allow for an accurate determination of the GCR energy differential fluxes at the top of the atmosphere. Conversely, experiments carrying magnetic spectrometers in space provide the needed observations. In [37], we reported the proton flux observed by the SMILI experiment during the FD of 5 September 1989. Unfortunately, the evident normalization problems between the MASS experiment proton data gathered before the FD and the SMILI experiment observations prevented us from correctly estimate the effects of the FD as a function of the energy. The PAMELA experiment carried out the first observation of proton and helium energy spectra in space before and during the FD of 14 December 2006 between 1650 and 2235 UT [30] without normalization uncertainties. In figure 5 of [30], it can be observed that during the FD, the proton flux appears depleted above 400 MeV, whereas below this energy, SEPs overcome the GCR flux. Unfortunately, helium flux observations were affected by statistical errors that masked the effects of the FD.

The SEP proton energy spectrum during the FD is well represented by a power-law trend with an exponential cut-off (top dot-dashed line in figure 1) [38]:

$$F_{SEPs}(E) = 58718\, E^{-0.37}\, e^{-\frac{E}{0.072}} \quad \text{Particles}/\left(\text{m}^2\ \text{sr}\ \text{s}\ \text{GeV}\right). \tag{5}$$

The GCR proton energy spectrum (bottom dot-dashed line in figure 1) was estimated by extrapolating the observed trend of high-energy measurements at low energies. This galactic proton component is parameterized as follows:

$$F_p(E) = 18000\,(E + 1.18)^{-3.68}\, E^{0.89} \quad \text{Particles}/\left(\text{m}^2\ \text{sr}\ \text{s}\ \text{GeV}\right). \tag{6}$$

It is worthwhile to note that the test-mass charging during this FD (see section 6) was estimated by considering the role of SEPs at low energies. The helium contribution as a fraction of proton charging can be inferred from the results reported in table 1 for the steady-state GCRs expected in 2015.

4. GCR variations induced by the Sun's rotation

The Sun is a sphere of plasma and gas rotating with a period of 25–26 days at the equatorial and near-equatorial regions and a period of 36 days near the poles. The solar rotation periodicity appears as 27–28 days to an observer on Earth due to the orbital motion of our planet and to the solar wind characteristics observed from Earth, representative of the conditions of the Sun's near-equatorial regions in the heliosphere. The overall GCR energy spectrum measured from Earth shows analogous 27 day intensity variations (A_{27}) induced by asymmetries in the electromagnetic field distribution in the interplanetary medium. Only rarely were different periodicities detected from Earth. In 2009, for instance, GCR variations of 34 day periods were observed, showing that at the onset of solar cycle 24, those processes

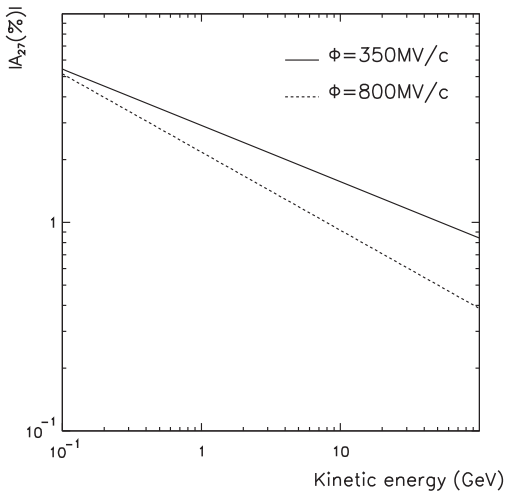

Figure 2. Parameterizations of 27 day GCR intensity fractional variations in 2015. Variations must be intended to be both positive and negative with respect to the average overall GCR observed intensity. Solid (ϕ = 350 MV/c) and dashed (ϕ = 800 MV/c) lines represent the maximum and minimum expected values, respectively.

causing the variations induced by the Sun's rotation occured at heliolatitudinal regions different than the equator. GCR 27 day maximum intensity variations measured from Earth are observed at solar minimum during positive polarity periods. Minimum variations are detected at solar maximum during negative polarity periods. Alania *et al* [39] found that the GCR 27 day minimum and maximum variation amplitudes (as a fraction of GCR flux) present a power-law spectrum in rigidity R as indicated next:

$$A_{27} = b\, R^{-\delta}. \tag{7}$$

This spectrum appears hard ($\delta = 0.54 \pm 0.11$) during positive polarity periods and soft ($\delta = 0.95 \pm 0.12$) during negative polarity epochs. Based on of these results, we have parameterized the absolute values of the 27 day variations as a function of proton kinetic energy (E_K) during the second half of 2015, under the minimum (ϕ = 350 MV/c; $|A_{27\,min}|$) and maximum (ϕ = 800 MV/c; $|A_{27\,max}|$) solar modulation conditions predicted for LISA-PF. These parameterizations are reported in equations (8) and (9) and displayed in figure 2 as a fractional amplitude variation of the average expected GCR intensity in 2015:

$$\left|A_{27\,min}\right|\ (\%) = 3.88\left(E_K^2 + 2 \times E_K \times 0.938\right)^{-\frac{0.54}{2}} \tag{8}$$

$$\left|A_{27\,max}\right|\ (\%) = 3.23\left(E_K^2 + 2 \times E_K \times 0.938\right)^{-\frac{0.75}{2}}. \tag{9}$$

The 27 day GCR variations are characterized by anisotropies smaller than 0.06% (0.03%) during positive (negative) polarity epochs, which that can be neglected for the estimate of the LISA-PF test-mass charging.

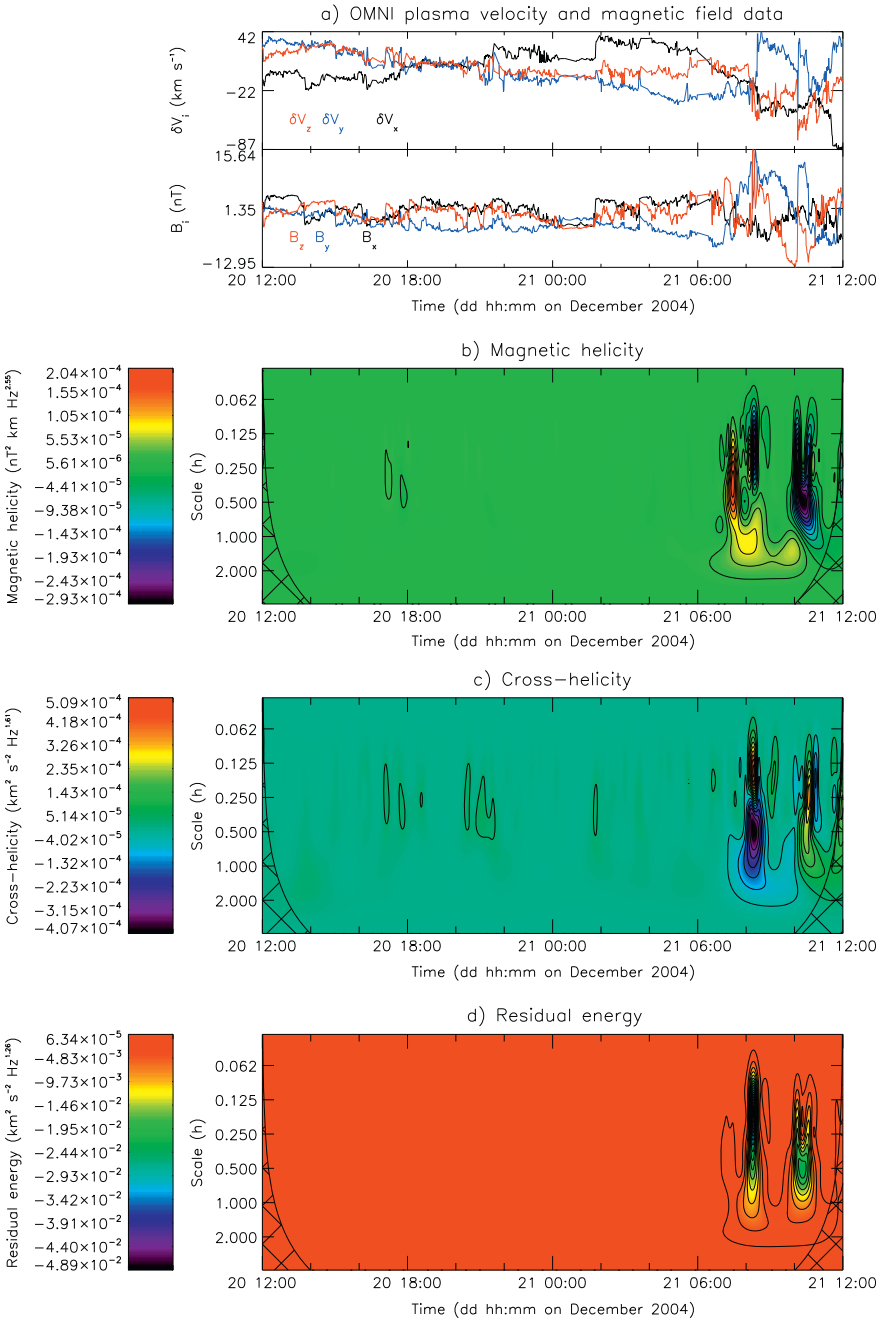

Figure 3. (a) Time profiles of the x, y, and z components (black, blue, and red curves, respectively) of the plasma velocity fluctuations and of the magnetic field (in the GSE coordinates) acquired by the WIND/SWE and WIND/MFI instruments, respectively, from 20 December 2004 at 12:00 UT to 21 December 2004 at 12:00 UT. (b) Magnetic helicity ($H_m^{(r)}$), (c) cross helicity (H_c), and (d) residual energy (E_r) compensated spectrograms. The continuous lines in the bottom panels are the COI and delimit cross-hatched areas where the estimations of $H_m^{(r)}$, H_c, and E_r are not fully reliable.

5. GCR variations in the LISA-PF frequency bandwidth

Small-amplitude GCR variations and fluctuations of the order of hours or minutes lie in the LISA-PF frequency band of interest (10^{-4} and 10^{-1} Hz) as a technology-testing mission for eLISA. To detect these GCR variations, experiments with large geometrical acceptances are required. Unfortunately, large geometrical factors are infeasible in experiments carrying magnetic spectrometers allowing for particle differential flux measurements. Precious clues on hourly GCR variations as a function of the energy were provided by the magnetic spectrometer balloon-borne experiment BESS-Polar I [33, 40], flown from 13 December to 21 December 2004 over Antarctica. BESS-Polar I carried out the measurement of the GCR proton flux between 0.46 and 100 GeV every 2 h [41]. During the entire period of the experiment, data taking the maximum observed variations of the proton energy differential flux in the rigidity range 1–2 GV/c was of ±5%, whereas above 5 GV, the South Pole neutron monitor count rate decreased 2%, indicating a GCR flux variation of a few percent. Maximum proton flux variations observed in the same two consecutive time bins in all energy intervals were 2%. This occurred after 6:00 a.m. 21 December 2004. We note that it is difficult to disentangle the role of the geomagnetic field in affecting GCR very short-term variations observed near Earth and it may be questioned whether identical variations could be reasonably expected for LISA-PF orbiting about L1. To this purpose, the study of three magnetohydrodynamic (MHD) invariants, namely the magnetic helicity, the cross helicity, and the residual energy, which are related to the magnetic field topology during the short-time reduction in the galactic proton flux observed by BESS-Polar I, is carried out in this paper. The magnetic helicity characterizes the knottedness of the magnetic field line [42], the cross helicity represents a measure of the degree of alignment between the magnetic field and the velocity field fluctuations, and finally, the residual energy quantifies the imbalance between kinetic and magnetic energies. When the power spectra of the kinetic and magnetic energies are considered, these three MHD quantities (with their normalized forms) can be defined in the frequency domain. Furthermore, the use of the wavelet transforms allows for the investigation of the magnetic helicity and cross helicity, as well as of the residual energy, not only in the frequency domain but also in time. It is thus possible to temporally localize magnetic structures in the solar wind with a characteristic magnetic helicity content, investigating the degree of alignment between the velocity and magnetic fluctuations embedded in the structure, and whether or not it is a magnetic or plasma structure, by quantifying the residual energy. The magnetic helicity, cross helicity and residual energy spectrograms obtained with the wavelet analysis can be properly compensated with power-law functions of the wave number. The wavelet decompositionwas successfully adopted in Telloni *et al* [43] and is used here. Data from the magnetic field investigation (MFI, for magnetic field components) [44] and the solar wind experiment (SWE, for velocity components and number density) [45] instruments onboard the Wind spacecraft were considered to compute the MHD rugged invariants. This technique was applied to the Wind 1-min data in L1, to investigate, in both time and temporal scales, τ ($\tau = 1/f$ where f is the frequency), the content of the magnetic helicity, the cross helicity, and the residual energy from 20 December 2004 at 12:00 UT to 21 December 2004 at 12:00 UT, thus encompassing the observed short-term variation in the GCR flux, as reported in figure 3.

The top panel displays the time profiles of the components of the plasma velocity fluctuations and of the magnetic field, with an average time resolution of 1 min, in the geocentric solar ecliptic (GSE) reference system. In that reference frame, the x-axis points towards the Sun and z-axis is perpendicular to the plane of the Earth's orbit around the Sun, so that at $x > 0$, clockwise (counterclockwise) rotations of the magnetic vector in the y-z plane perpendicular to the sampling direction are observed to have positive (negative) magnetic helicity. figures 3(b)–(d) show the compensated spectrograms (up to temporal scales larger

than 4 h) of the magnetic helicity, cross helicity and residual energy, respectively. The cross-hatched areas below the cones of influence (COI) line (represented as a continuous line in the panels) indicate the regions of the spectrograms where edge effects, due to the finite length of the time series, are not negligible; thus, only the features above the (COI) (i.e., at shorter scales) are fully reliable. Data reported in figure 3 are compatible with the possibility that a flux rope caused the GCR depression observed by BESS-Polar I. Flux ropes are magnetic structures of the solar wind characterized by a large amplitude, smooth rotation of the magnetic field vector, by an enhanced magnetic field strength, and by a low level of both proton density and temperature with respect to the surrounding plasma, exhibiting scale sizes typically of about 0.01 AU and temporal duration of the order of few hours, as detected at 1 AU [46–48]. These structures are modeled as a cluster of magnetic field lines bended into a tube-like shape having a strong axial symmetry, the magnetic field far from the axis being weak and azimuthal [49].

Analogous findings and results were found by Quenby *et al* ([50, 51] and references therein). These authors studied spatially localized GCR short-term variations using data collected with the high sensitivity telescope HIST aboard Polar and the large area anticoincidence shield (ACS, ACSSAT) and the saturated counts of Ge detector system (GEDSAT) aboard Integral. The proton fluence above 100 MeV was measured on Polar, whereas the overall particle triggers above 100 keV and GCR fluence above 150 and 200 MeV were observed aboard Integral. Polar was launched on 24 February 1996. Operations ended on 28 April 2008. The spacecraft was in a highly elliptical (86 degrees) inclination orbit with a period of 17.5 h with apogee of 9 R_E (56000 km) and perigee of 2 R_E (11500 km). Integral was launched on 17 October 2000. Mission operations end is expected in 2016. Integral is placed into a geosynchronous highly eccentric orbit (51.6 degrees inclination) with perigee of 9000 km and apogee of 153000 km (28 R_E). Five-minute sums of one-second data above 100 keV, 100 MeV, and 200 MeV gathered aboard the Integral satellite presented a similar trend as a function of time except for spikes in the lower energy bin due to magnetospheric electrons easy to identify and remove. The observed maximum GCR variations in a 10 h time interval was 1.7%. The same authors found maximum variations of 5% in the trend on the proton intensity gathered by HIST aboard Polar in the frequency range 10^{-6} Hz–10^{-3} Hz. We conclude that GCR short-term variations in the frequency band of interest of LISA-PF bandwidth (10^{-4} Hz–10^{-1} Hz) observed at various distances from Earth are of the order of magnitude of 2–3% and therefore, the BESS-Polar I data can be safely used to study the test-mass charging variations in the L1 Lagrange point.

6. LISA-PF test-mass charging during the mission operations

We have carried out the simulation of the LISA-PF test-mass charging with the Fluka Fortran-based Monte Carlo package [20, 21]. GCR particles were propagated through the LISA-PF spacecraft by assuming an isotropic particle distribution. The spacecraft geometry (shown in figure 4) was written in C^{++} programming language for the Geant4 simulation toolkit (see [52] for details). To redirect the Fluka geometry routines to Geant4 geometry methods, we used the FLUGG interface, which provides a library of proper wrappers. The implementation of the same spacecraft geometry in two different Monte Carlo programs allows us to compare the simulation outcomes when the same particle energy spectra are considered in input. In case of agreement, the other results presented here for the first time can be considered validated.

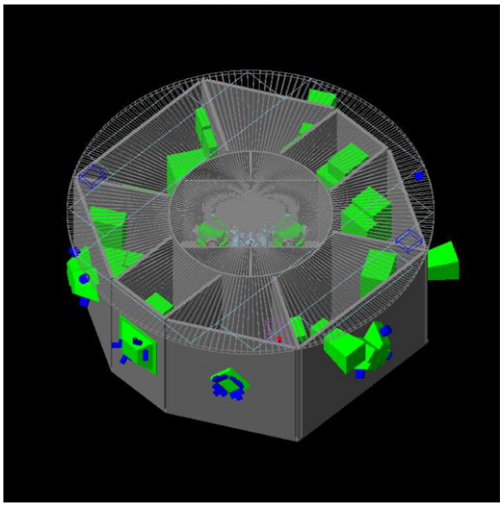

Figure 4. Sketch of the LISA-PF geometry.

We have studied the average test-mass net (λ_{net}) and effective (λ_{eff}) charging due to GCR proton and helium nuclei during the LISA-PF mission operations. The net charging rate deposited in the test masses is represented by the following equation:

$$\lambda_{net} = \sum_{j=-\infty}^{+\infty} j\lambda_j \quad \text{e s}^{-1} \tag{10}$$

where j represents the amplitude of charging released by single events and λ_j is the rate of occurrence of these events. Positive and negative charges cancel out in the net charging computation although both contribute to the effective charging rate defined next:

$$\lambda_{eff} = \sum_{j=-\infty}^{+\infty} j^2\lambda_j \quad \text{e s}^{-1}. \tag{11}$$

where λ_{eff} represents the charging of single charges that would generate the same observed shot noise. The spectral density of the charging shot noise is expressed in terms of the effective charging rate:

$$S = \sqrt{2e^2\lambda_{eff}} \quad \text{e s}^{-1}\, Hz^{-1/2}. \tag{12}$$

The charging fluctuations at frequency f are represented by

$$S_Q(2\pi f) = \frac{S}{2\pi f} = \frac{\sqrt{2e^2\lambda_{eff}}}{2\pi f} \quad \text{e Hz}^{-1/2}. \tag{13}$$

For each considered case study of the test-mass charging simulation, we propagated more than 2×10^6 primary particles through the LISA-PF spacecraft. This choice allows us to optimize the computing time by limiting the uncertainty on the λ_{net} and λ_{eff} below 5 and 2%, respectively. In particular, we aim to maintain the uncertainty on the λ_{eff} below the expected fluctuations of this parameter generated by GCR short-term variations.

Table 4. LISA-PF net (λ_{net}) and effective (λ_{eff}) test-mass charging and charging shot noise spectral density (S) induced by GCR protons (p) and helium isotopes (He^3, He^4). Minimum (min) and maximum (max) expected particle fluxes in 2015 are considered. The effects of a Forbush decrease (FD 14/12/2006) on the test-mass charging with respect to steady-state conditions prior the event (11/2006), 27 day positive (+) and negative (−) variations with respect to the average proton GCR flux and 2 h proton flux reduction are also reported for minimum and maximum proton flux projections. Typical uncertainties of 5 and 2% should be considered on λ_{net} and λ_{eff}, respectively.

Particle	λ_{net} (e^+/s)	λ_{eff} (e/s)	S (e s^{-1} $Hz^{-1/2}$)
p_{min}	14.1	168.9	18.4
p_{max}	32.5	295.5	24.3
He^3_{min}	0.22	0.92	1.4
He^3_{max}	1.9	5.6	3.4
He^4_{min}	0.81	1.9	2.0
He^4_{max}	3.8	10.7	4.6
$p_{11/2006}$	31.2	312.6	25.0
$p_{FD14/12/2006}$	19.4	213.1	20.6
$p_{27-day+;\,min}$	16.6	176.2	18.8
$p_{27-day-;\,min}$	10.9	173.7	18.6
$p_{27-day+;\,max}$	35.8	250.0	22.4
$p_{27-day-;\,max}$	27.1	239.7	21.9
$p_{2\,h\,min}$	11.5	176.6	18.8
$p_{2\,h\,max}$	30.0	231.1	21.5

In table 4, we have reported the net and effective charging induced by GCRs when maximum (p_{max}, He^3_{max} and He^4_{max}) and minimum (p_{min}, He^3_{min} and He^4_{min}) energy spectrum projections are considered.

Estimated minimum and maximum charging shot noise induced by protons and helium nuclei on LISA-PF test masses are 18.4 and 24.3 e $s^{-1}Hz^{-1/2}$, respectively. This result appears in excellent agreement with that of 24.9 e $s^{-1}Hz^{-1/2}$ obtained with the Geant4 simulation toolkit [52] when solar minimum conditions were assumed ($\phi \simeq 350$ MV/c). The minimum expected shot noise at the time of LISA-PF was never estimated before.

A Forbush decrease like that dated 14 December 2006 would have reduced the LISA-PF test-mass charging by 30% in less than 1 d with respect to the pre-existing situation (November 2006). GCR short-term variations of small intensity (27 day variations and variations in the LISA-PF bandwidth) affect mildly the test-mass charging. We will be able to monitor GCR intensities variations down to half-an-hour periodicities with the use of the particle detectors, as described in the following section.

7. Observations of GCR short-term variations with LISA-PF radiation monitor

7.1. LISA-PF particle detector

A particle detector for proton and helium nuclei monitoring will be hosted on LISA-PF [16, 17]. This device will be placed behind the spacecraft solar panels and oriented along the Sun–Earth direction. The radiation monitor consists of two 1.4 × 1.05 cm^2 area silicon wafers

of 300 μm thickness, placed in a telescopic arrangement separated by 2 cm. A shielding, copper box surrounds the silicon wafers. The box thickness is 6.4 mm. The radiation monitor will provide the counting rate of particles crossing each silicon layer and ionization energy losses of particles traversing both silicon wafers (coincidence mode). For particle energies > 100 MeV/n, the radiation monitor geometrical factor is found to be energy independent and equal to 9 cm^2 sr for particle isotropic incidence on each silicon wafer. In coincidence mode, the geometrical factor is about one-tenth of this value. During the LISA-PF mission, the radiation monitor data will be stored in the form of histograms over periods of 600 s and then sent to the onboard computer. The maximum allowed radiation monitor counting rate is 6500 counts/s on both silicon wafers, corresponding to an event integrated proton fluence of 10^8 protons/cm^2 at energies > 100 MeV. In coincidence mode, up to 5000 energy deposits per second can be stored in the histogram. The occurrence of events of this intensity is quite rare. The expected number of SEP events with fluence > 10^8 protons/cm^2 at energies > 30 MeV, for instance, is less than 1 per year [53]. Even in case of radiation monitor saturation, we would be able to follow the dynamics of SEP events and the solar particle spatial distribution onboard LISA-PF if GCR and SEP energy differential fluxes will be provided by other experiments.

The radiation monitor placed on LISA-PF and those onboard future space interferometers will provide precious, *in situ* observations for space weather applications and solar physics investigations, as it was pointed out in [54, 55].

7.2. Measurements of GCR short-term variations onboard LISA-PF

GCR fluctuations in the LISA-PF bandwidth are spatially localized and therefore measurements gathered far from the spacecraft are useless to investigate their role in the test-mass charging.

When there is no occurrence of SEP events, the radiation monitor provides the integral flux of p and He nuclei of galactic origin (> 100 MeV/n). The signal (S) to noise (N) ratio for a quasi-periodic signal can be expressed by

$$\frac{S}{N} \simeq \frac{A}{\sigma_A}\sqrt{N} \tag{14}$$

where A represents the amplitude of the signal, σ_A is the measurement error on A, and N is the number of observations. When the S/N ratio for the particle countrate in the LISA-PF radiation monitor is estimated, A represents the countrate in each time interval (ΔT) and σ_A represents the Poisson error of the countrate in the same time interval. In the case the overall GCR spectrum intensity variation lasts for more than one interval of time, the S/N ratio improves as $\sqrt{N_{\Delta T}}$. Short-term GCR variations of 2% would be detected in half-an-hour time in case of maximum estimated GCR intensity in 2015. One hour would be needed in case of minimum estimated GCR intensity in 2015.

8. Conclusions

We have estimated the LISA-PF test-mass charging due to GCRs in 2015 with the fortran-based Fluka Monte Carlo toolkit. Minimum and maximum GCR energy spectrum projections during the LISA-PF operations in 2015 were estimated. Steady-state GCR fluxes and short-term variations were considered. In particular, we studied the Forbush decrease of 14 December 2006, the GCR 27 day variations and, finally, the GCR fluctuations in the LISA-PF bandwidth. We have found that minimum and maximum charging shot noise to be expected

at steady-state range between 18.4 and 24.3 e $s^{-1}Hz^{-1/2}$, respectively. An excellent agreement was found with the simulation carried out at solar minimum conditions with the GEANT Monte Carlo toolkit. A reduction of test-mass charging shot noise of approximately 30% is expected during a FD. GCR short-term variations in the LISA-PF bandwidth do not generate remarkable changes in the test-mass charging. GCR short-term variations will be detected on LISA-PF with data from particle detectors down to a minimum of half-an-hour periodicities.

Acknowledgments

This work was financially supported by the Italian Space Agency within the Study Exploration of the Solar System program under contract ASI–INAF I/05/07/0. IM and CG acknowledge support from the Spanish Research Ministry, contract AYA2010-15709.

References

[1] Jenrich O *et al* (eLISA/NGO Collaboration) 2012 *NGO Assessment Study Report Yellow Book*
[2] Amaro Seoane P *et al* (The eLISA Consortium) 2013 arXiv:1305.5720
[3] Antonucci F *et al* 2011 *Class. Quantum Grav.* **28** 094002
[4] Antonucci F *et al* 2012 *Class. Quantum Grav.* **29** 124014
[5] Araújo H M *et al* 2005 *Astropart. Phys.* **22** 451–69
[6] Grimani C 2005 *Class. Quantum Grav.* **22** 327–32
[7] Shaul D 2006 *AIP. Conf. Proc.* **873** 172–8
[8] Papini P, Grimani C and Stephens A S 1996 *Nuovo Cimento* **19** 367–87
[9] Astone P *et al* 2001 *Phys. Lett.* B **499** 16–22
[10] Astone P *et al* 2002 *Phys. Lett.* B **540** 179–84
[11] Astone P *et al* 2008 *Astropart. Phys.* **30** 200–8
[12] Ronga F *et al* 2012 *J. Phys.: Conf. Ser.* **375** 062006
[13] Yamamoto K *et al* 2008 *Phys. Rev.* D **78** 022004
[14] Andretta V *et al* 2014 *Proc. SPIE* **9152**, *Software and Cyberinfrastructure for Astronomy III, 91522Q (18 July 2014)* doi:10.1117/12.2055158
[15] Grimani C *et al J. Phys.: Conf. Ser.* submitted
[16] Cañizares P *et al* 2011 *Class. Quantum Grav.* **28** 094004
[17] Mateos I *et al* 2012 *J. Phys.: Conf. Ser.* **363** 012050
[18] Grimani C *et al* 2012 *Class. Quantum Grav.* **29** 105001
[19] Forbush S E 1937 *Phys. Rev.* **51** 1108–9
[20] Battistoni G, Muraro S, Sala P R, Cerutti F, Ferrari A, Roesler S, Fassó A and Ranft J 2007 *The FLUKA code: description and benchmarking, Proc. Hadronic Shower Simulation Workshop, 2006, Fermilab 6–8 September 2006* (*AIP Conf. Proc.* **896**) ed M Albrow and R Raja pp 31–49
[21] Ferrari A, Fassó A, Ranft J and Sala P R 2005 *FLUKA: a Multi-Particle Transport Code, CERN 2005–2010*
[22] Grimani C *et al* 2009 *Class. Quantum Grav.* **26** 215004
[23] Grimani C *et al* 2014 *Class. Quantum Grav.* **31** 045018
[24] http://solarscience.msfc.nasa.gov/predict.shtml
[25] http://wso.stanford.edu/gifs/Polar.gif
[26] Grimani C *et al* 2007 *Proc. 30th Int. Cosmic Ray Conf. (Merida)* **1** 485–8
[27] Gleeson L J and Axford W I 1968 *Ap. J.* **154** 1011–26
[28] Grimani C *et al* 2009 *Class. Quantum Grav.* **26** 094018
[29] Shikaze Y *et al* 2007 *Astrop. Phys.* **28** 154–67
[30] Adriani O *et al* 2011 *Astrophys. J.* **742** 102
[31] Usoskin I G *et al* 2005 *J. Geophys. Res.* **110** A12108
[32] Casolino M *et al* 2011 *Astrophys. Sp. Sci. Trans.* **7** 465–9
[33] Abe K *et al* 2014 Time variations of cosmic-ray helium isotopes with BESS-Polar I *Adv. Space Res.* **53** 1426–31
[34] Kojima H *et al* 2013 *Proc. 33rd Int. Cosmic Ray Conf. (Rio de Janeiro)*

[35] Abbrescia M *et al* 2011 *Eur. Phys. J. Plus* **126** 61
[36] Usoskin I G *et al* 2008 *J. Geophys. Res.* **113** A07102
[37] Grimani C *et al* 2011 *Class. Quantum Grav.* **28** 094005
[38] Grimani C *et al* 2012 *J. Phys. Conf. Ser.* **363** 012045
[39] Alania M V, Gil A and Modzelewska R 2008 *Astrophys. Sp. Sc. Trans.* **4** 31–34
[40] Hams T *et al* 2009 *Proc. 31st Int. Cosmic Ray Conf. (Łódź)*
[41] Thakur N *et al* 2011 *Proc. 32nd Int. Cosmic Ray Conf. (Beijing)* **11** 222
[42] Moffat H K 1978 *Magnetic Field Generation in Electrically Conducting Fluids* (Cambridge: Cambridge University Press)
[43] Telloni D *et al* 2008 *Astrophys. J.* **751** 19
[44] Lepping R P *et al* 1995 *Space Sci. Rev.* **71** 207–29
[45] Ogilvie K W *et al* 1995 *Space Sci. Rev.* **71** 55–77
[46] Moldwin M B *et al* 1995 *J. Geophys. Res.* **100** 19903–10
[47] Moldwin M B *et al* 2000 *Geophys. Res. Lett.* **27** 57–60
[48] Feng H Q *et al* 2007 *J. Geophys. Res.* **112** A02102
[49] Russell C T and Elphic R C 1979 *Nature* **279** 616–8
[50] Quenby J J *et al* 2008 *J. Geophys. Res.* **113** A10102
[51] Quenby J J *et al* 2013 *Adv. Astron.* **2013** 429303
[52] Wass P *et al* 2005 *Class. Quantum Grav.* **22** 311–7
[53] Storini M *et al* 2008 *OPOCE publisher for COST 724 action* 63–69
[54] Grimani C and Vocca H 2005 *Class. Quantum Grav.* **22** 333–8
[55] Braxmaier C *et al* 2012 *Exp. Astron.* **34** 181–201